K = adsorption equilibrium constant, cm^3/g
N = diffusive flux, g-mole/(cm^2)(s)
N_T = total diffusive flux in bidisperse pellet, g-mole/(cm^2)(s)
n = concentration of adsorbate on surface, g-mole/g
R = pellet radius, cm
r_{eff} = effective radius for micropore diffusion in bidisperse pellet, cm
t = time, s
t_{obs} = observed time for equalization of concentration gradient in pellet, s; t_M, t_μ = equalization times for macro and micropores, respectively
x = coordinate in the direction of diffusion, cm

Greek Letters

δ = tortuosity factor
ϵ = porosity; ϵ_M and ϵ_μ denote void fractions in macro and micropores, respectively
ρ_p = density of bidisperse pellet, g/cm^3
$\rho_{p\mu}$ = density of microporous particle in pellet, g/cm^3

LITERATURE CITED

Antonson, C. R., and J. S. Dranoff, "The Kinetics of Ethane Adsorption on Molecular Sieves," *Chem. Eng. Progr. Symp. Ser. No. 74*, 61 (1967).

———., "Nonlinear Equilibrium and Particle Shape Effects in Intraparticle, Diffusion-Controlled Adsorption," *ibid.*, No. 96, 20 (1969).

———., "Adsorption of Ethane on Type 4A and 5A Molecular Sieve Particles," *ibid.* 27.

Eberly, P. E., "Adsorption of Normal Paraffins in Erionite and 5A Molecular Sieves," *Ind. Eng. Chem. Product Research Develop.*, **8**, 140 (1969).

———., "Diffusion Studies in Zeolites and Related Solids by Gas Chromatographic Techniques," *Ind. Eng. Chem. Fundamentals*, **8**, 25 (1969).

Kallenbach, R., and E. Wicke, "Die Oberflaechen diffusion von Kohlendioxyde in Aktiven Kohler," *Kolloid-Z*, **97**, 135 (1941).

Johnson, M. F. L., and W. E. Stewart, "Pore Structure and Gaseous Diffusion in Solid Catalysts," *J. Catalysis*, **4**, 248 (1965).

Kawazoe, K., and Y. Fukuda, "Studies on Solvent Recovery by Activated Carbon," *Kagaku Kogaku*, **29**, 374 (1965).

Kondis, E. F. and J. S. Dranoff, "Kinetics of Isothermal Sorption of Ethane on 4A Molecular Sieve Pellet," *Ind. Eng. Chem. Process Design Develop.*, **10**, 109 (1971).

Mitani, M., and S. Hami, "Research on Gaseous Diffusion Phenomena in Various Porous Catalysts—Measurement of Effective Diffusion Coefficient by Frontal Chromatography," *Kagaku Kogaku*, **34**, 1087 (1970).

Padberg, G., and J. M. Smith, "Chemisorption Rates by Chromatography," *J. Catalysis*, **12**, 172 (1968).

Rao, M. Raja, and J. M. Smith, "Diffusion Resistances in Alumina and Silica Catalysts," *AIChE J.*, **9**, 485 (1963).

Ruckenstein, E., A. S. Vaidyanathan, and G. R. Youngquist, "Sorption by Solids with Bidisperse Pore Structures," *Chem. Eng. Sci.*, **26**, 1305 (1971).

Sargent, R. W. H., and C. J. Whitford, "Diffusion of Carbon Dioxide in Type 5A Molecular Sieve," *Molecular Sieves Zeolites II*, Am. Chem. Soc. (1971).

Satterfield, C. N., and W. G. Margretts, "Diffusion in Sodium Mordenite," *AIChE J.*, **17**, 295 (1971).

Wakao, N., and J. M. Smith, "Diffusion in Catalyst Pellets," *Chem. Eng. Sci.*, **17**, 825 (1962).

Manuscript received August 29, 1972; revision received October 16, 1972; paper accepted October 27, 1972.

Description of Meniscus Profiles in Free Coating II—Analytical Expressions

CHIE Y. LEE and JOHN A. TALLMADGE

Department of Chemical Engineering
Drexel University, Philadelphia, Pennsylvania, 19104

The authors are interested in describing the location of curved interfacial boundaries arising in dynamic menisci and in describing the profiles in terms of meniscus thickness h—as a function of laboratory position x (Lee and Tallmadge, 1972a). In a recent study, profile data were obtained for the case of free coating on a flat sheet over a range of speeds and bath depths (Lee and Tallmadge, 1972b). The purpose of this note is to describe the previously obtained profiles with analytical expressions for $h(x)$ and to present quantitatively the influence of speed and bath depth on the analytical parameters.

For free coating, we take x as the distance above the bath surface and note that the meniscus thickness decreases asymptotically up to a constant thickness h_0. Using $\lambda \equiv x/h_0$ and $L \equiv h/h_0$, the meniscus profile becomes $L(\lambda)$, where the thickness L decreases from a large value at the bath surface ($\lambda = 0$) to L of 1 at a large height λ. Some typical data are shown in Figure 1; the bath depths in Figure 1 are about 30 h_0 so that these data are called deep bath profiles. The coating speed U_w is given in terms of the nondimensional capillary number Ca which equals $U_w(\mu/\sigma)$. Figure 1 shows that meniscus profiles have two linear regions on this semilog plot, with a division near L of 2 to 3. The data can therefore be described by a linear analytical expression for each region of upper and lower meniscus. Exponential forms of these two expressions are

$$\text{Upper:} \quad (L < 2) \qquad L = 1 + B_1 \exp(-\lambda/M_1) \tag{1}$$

$$\text{Lower:} \quad (L > 2) \qquad L = 1 + B_2 \exp(-\lambda/M_2) \tag{2}$$

The M values represent the slopes in Figure 1 and the B values represent intercepts with the horizontal axis.

In repeatability tests using the same photographs, it was found that slopes did not vary appreciably, so that slopes do not appear to be sensitive to the experimental

Correspondence concerning this note should be addressed to J. A. Tallmadge. C. Y. Lee is with Pennwalt Corporation, Warminster, Pennsylvania.

technique. However, uncertainties in λ (and thus intercepts B) were found to be noticeable in these repeatability tests—varying from about 0.1 to 0.9 and averaging about 0.2 to 0.3. Uncertainties in λ reflect the uncertainty in determining the bath surface position precisely. Small viscosity changes, due to the small temperature changes from run to run, were calculated using

$$\ln(\mu/\mu_0) = \exp[6890\,(t_0 - t)/(t)\,(t_0)] \qquad (3)$$

Here t is degrees K, the reference temperature t_0 is 299.7°K, and the reference viscosity was 1.31 N-s/m². The constant in Equation (3) was determined using data at four temperatures; namely the reference temperature plus about 15, 21, and 33°C.

DEEP BATH PROFILES

Deep bath data were obtained at the six speeds (six Ca) and conditions shown in Table 1. The measured entrainment values shown in Table 1 include the constant thickness h_0 for each run, the flow rate w, and the nondimensional forms of each, given by $T_0 \equiv h_0\,(\rho g/\mu U_w)^{1/2}$ and $Q = (w/\rho b U_w)\,(\rho g/\mu U_w)^{1/2}$. Comparison of Q obtained from flow data (Q_w) with that from thickness data (Q_0), as shown in Table 1, indicates good agreement, consistent data, and therefore the high precision of the h_0 value.

Of the six meniscus profiles measured, three are shown

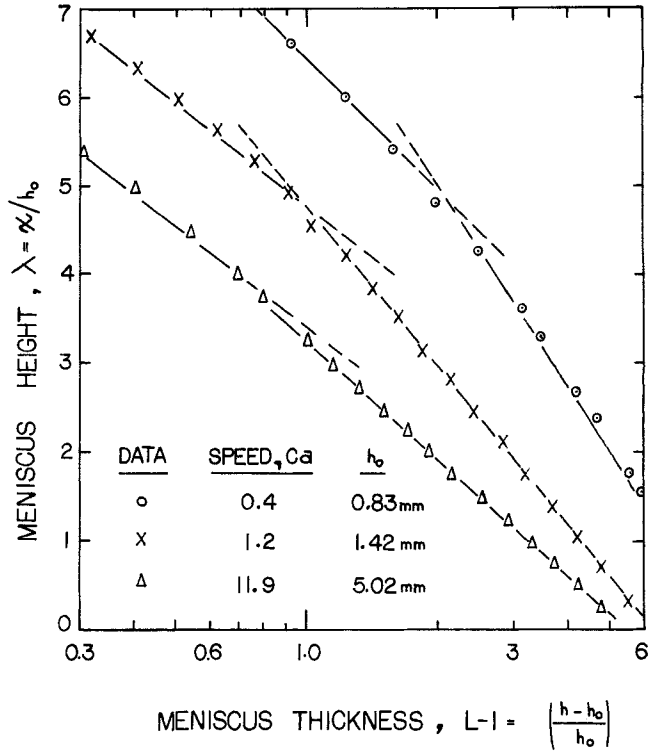

Fig. 1. Deep bath profiles for three coating speeds.

TABLE 1. DEEP BATH CONDITIONS, SLOPES AND INTERCEPTS

Speed, Ca	0.43	1.17	2.75	5.66	11.9	23.9
Conditions						
Speed, U_w, mm/s	12.7	33.1	74	161	331	666
Liquid temp, °C	28.9	28.3	27.7	28.4	28.1	28.1
Bath depth, d, mm	40	60	92	140	200	200
Run no.	B312	B309	B306	B304	B302	B301
Entrainment Data						
Thickness, h_0, mm	0.831	1.42	2.39	3.43	5.02	7.01
Thickness, T_0	0.654	0.676	0.744	0.743	0.749	0.739
Flow rate, w, g/s	0.49	2.17	7.71	25.2	73.4	207
Flow rate, Q_w	0.554	0.569	0.588	0.617	0.603	0.597
Flow rate, Q_0	0.561	0.573	0.607	0.606	0.609	0.604
Difference in Q	+1%	+1%	+3%	−2%	+1%	+1%
Upper Meniscus ($L < 2$)						
Slope M_1	2.22	1.70	1.40	1.52	1.65	1.83
Intercept B_1	18.5	16.5	14.0	8.5	7.8	11.7
L Range	1.2/3	1.2/2	1.2/2	1.1/3	1.1/2	1.2/2
λ Range	10/5	7/5	6/4	6/2	7/4	7/4
Lower Meniscus ($L > 2$)						
Slope M_2	3.17	2.48	1.93	2.01	1.88	2.70
Intercept B_2	9.6	6.4	6.8	5.8	5.6	5.8
L Range	3/10	2/6	2/7	3/6	2/6	2/6
λ Range	4/0.6	4/0.4	3/0.3	3/0.2	3/0.2	4/0.3
Complete Profile (*)						
Slope M_3	1.36	1.14	0.92	0.72	1.08	1.05
Intercept B_3	8.9	10.1	7.2	2.7	2.3	6.6
Extreme Deviation (*)						
Location (−) in L	3.0	1.7	2.1	2.9	1.5	2.2
Location (+) in L	7.6	4.2	6.4	5.4	3.2	4.4
Extremum (−), %	5	7	6	5	4	5
Extremum (+), %	7	12	7	4	2	6

(*) This complete profile, given by Equation (4), has four parameters—M_1, B_1, M_3, and B_3 above. The deviation (between the photographic data and the analytical expression) has plus and minus extremums which occur at the L locations shown above.

in Figure 1. Profiles for Ca of 3, 6, and 24 are not shown because of overlap with those on the graph. For example, the magnitude of the $Ca = 24$ profile in λ $(L - 1)$ form is similar to that shown for Ca of 1 in Figure 1 and the magnitudes of the Ca 3 and Ca 6 profiles are similar to that shown for Ca of 12 in Figure 1. This overlap, which is due to the different dependence of $h(x)$ and h_0 on Ca for the conditions studied, does not appear on a dimensional plot of $h(x)$.

Analytical expressions for the six profiles were developed for both the upper and lower meniscus and are shown as the M_1, B_1, M_2, and B_2 parameters of Table 1. It is seen that the lower slope is larger than the upper slope and that slopes above Ca of 1 are a weak function of Ca. The lower intercept (B_2) is approximately the same as the B value obtained by data and is approximately constant at Ca above 1.

SHALLOW BATH PROFILES

At each speed, shallow bath data were also obtained at three other depths. Thus the influence of depth was studied using four depths at each speed. Profile data for two typical speeds are shown in Figure 2 (Ca near 1.2) and Figure 3 (Ca near 12). Entrainment data and other data necessary to define conditions for the shallow-bath runs in these figures are given in Table 2. As before, the consistency test data, given by Q_w and Q_0 in Table 2, indicate generally good agreement and thus high precision of the h_0 thickness value.

For Ca near 1, Figure 2 shows that both the upper slope M_1 and lower slope M_2 were approximately constant over a wide range of bath depths, but that the intercepts B_1 and B_2 varied considerably with depth. Figure 3 shows that similar results, for both slopes and intercepts, were also found at a higher Ca near 12. Figures 2 and 3 are also typical of the sequences at the 4 other speeds.

Quantitative values of slopes were obtained for each of the 18 shallow bath runs, as shown by typical results in Table 2. Comparison of the slopes in Table 2 with Table 1 for the same speed shows the relative constancy for a given speed and the size of the small variations; at Ca near 1.2 for example, M_1 had values of 1.70, 1.70, 1.76, and 1.61 at decreasing depths.

The slopes of all 24 runs were then studied in sequences of four depths each. Within the 5 to 10% uncertainty in slope, results indicated no appreciable influence of bath depth on either slope. Because of this result, slopes M_1 and M_2 were averaged for each Ca. Table 3 shows that, for Ca above one, the average slopes are weak functions of Ca and that the overall average slope is about 1.6 and 2.2 for the upper and lower meniscus.

Quantitative values of both intercepts (B_1 and B_2) were also obtained for each shallow-bath run. Table 3 presents the values for each of the 20 runs for Ca above 1. Table 3 shows that the lower meniscus intercepts are substantially influenced by depth for shallow baths; because they are not functions of Ca, however, average values for each depth are given in Table 3.

The 20 values of upper meniscus intercepts (B_1) given in Table 3 appear to be functions of both depth and Ca; therefore, no averaging or simplification of the upper intercept dependence is suggested at this time. Some variation in B_1 may be due to uncertainty, however, because B_1 appears to be more sensitive to random experimental errors. At very small depths, where $d/h_0 \cong 4$, there is a larger uncertainty in h_0 as shown by entrainment checks.

For all 4 runs at Ca near 0.4, the slopes and intercepts obtained were in general higher than those for Ca above 1 and are therefore not included in Table 3. One example can be seen by comparing the results for the first run in Table 1 with the results for the other eleven runs (Tables 1 and 3).

COMPLETE, ONE-EQUATION PROFILES

The expressions given above have the advantage of showing the dependence on speed and bath depth in terms of parameters with physical meaning. However, the profile expressions were split into two equations for the upper and lower meniscus, as shown by Equations (1) and (2). Furthermore, the above expressions do not describe the region from L of 2 to 4 very accurately because the expressions were not continuous (complete) profiles throughout the entire $L(\lambda)$ regions. The purpose of this section is to present complete profiles using a one-equation approach, together with quantitative description of deviations and discussion of the new parameters developed.

Because Equation (1) also has a theoretical basis (Deryagin and Levi, 1964; Tallmadge, 1973), an attempt was made to extend it to include the lower meniscus. Using a semilog correction suggested earlier for one run (Lee and Tallmadge, 1972a), we have, by extension

$$L = 1 + B_1 \exp(-\lambda/M_1) - B_3 \exp(-\lambda/M_3) \quad (4)$$

Equation (4) was evaluated for each of the 24 profiles as follows. First, for each run, one pair of parameters (M_1 and B_1) were taken from the upper meniscus results presented above. Then the second pair of parameters (M_3 and B_3) were determined using a semilog plot of residuals, which were found to be linear. Typical parameters for Equation (4) are shown at the bottom of Table 1 for the six deep bath profiles. Maximum deviations in thickness L were within 7% for most profiles, which is considered good agreement with the data, especially for the lower meniscus region where L values are large. This one-equation approach is therefore suitable for describing

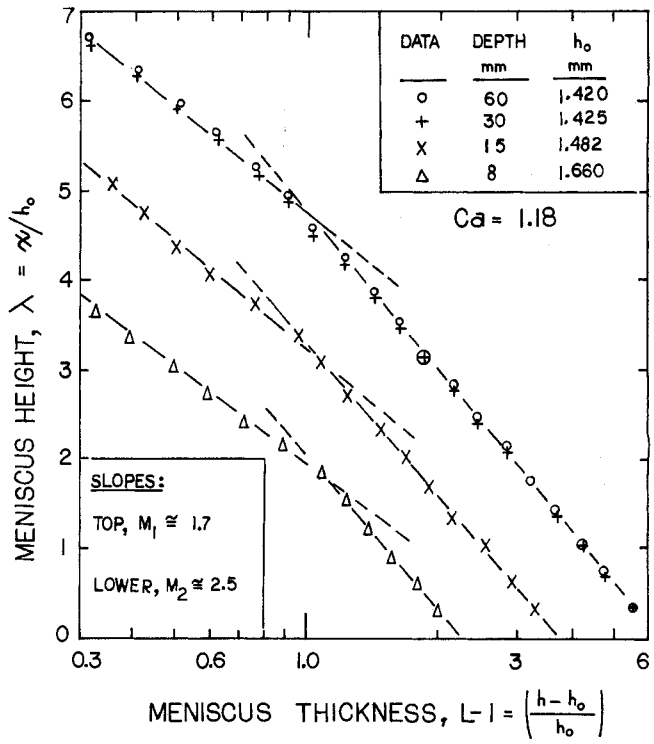

Fig. 2. Effect of bath depth on profiles at Ca near 1.

experimental L precisely for any one run.

As seen in Table 1, the M_3 slopes were found to be smaller than M_1 slopes, for the same conditions. Thus the M_3 correction term tends to become negligible at large λ, as desired. Therefore Equation (4) reduces to Equation (1) at large λ, which is the proper limiting behavior. The B_3 value was found to be approximately equal to the difference between the B_1 and B_2 terms, as expected. See Table 1. This is the proper limiting behavior at small λ.

Equation parameters for shallow baths indicate similar maximum deviations for any given run. A few sample values are shown in Table 2. However, the M_3B_3 parame-

Table 2. Shallow Bath Conditions at Two Ca

Speed, Ca	1.19	1.18	1.17	11.6	11.7	10.9
Conditions						
Speed, U_w, mm/s	36.4	36.8	37.0	334	333	335
Liquid temp, °C	29.3	29.6	29.8	28.5	28.4	29.4
Bath depth, d, mm	30	15	8	100	50	25
Run no.	B315	B320	B323	B305	B310	B316
Entrainment Data						
Thickness, h_0, mm	1.425	1.482	1.660	5.17	5.46	5.67
Thickness, T_0	0.672	0.703	0.791	0.780	0.823	0.885
Flow rate, w, g/s	2.38	2.44	2.47	75.2	76.4	76.1
Flow rate, Q_w	0.563	0.573	0.580	0.620	0.630	0.646
Flow rate, Q_0	0.571	0.587	0.626	0.622	0.637	0.654
Difference in Q	+1%	+2%	+8%	+1%	+1%	+1%
Upper Meniscus ($L < 2$)						
Slope M_1	1.70	1.76	1.61	1.56	1.52	1.45
Intercept B_1	16.5	6.2	3.3	7.8	5.4	4.0
L Range	1.2/2	1.2/2	1.2/2	1.2/2	1.2/2	1.2/2
λ Range	7/4	6/3	4/2	6/3	5/3	4/2
Lower Meniscus ($L > 2$)						
Slope M_2	2.47	2.45	2.53	2.02	1.97	2.10
Intercept B_2	6.4	3.8	2.3	5.0	3.7	2.7
L Range	2/6	2/4	2/3	2/6	2/4	2/3
λ Range	2/0.3	3/0.3	4/0.3	3/0.3	2/0.2	2/0.2
Complete profile (*)						
Slope M_3	1.14	0.92	0.70	0.88	0.77	0.62
Intercept B_3	10.1	2.5	1.1	2.8	1.8	1.3
Extreme Deviations (*)						
Location (−), in L	1.8	1.9	2.1	1.7	1.9	1.9
Location (+), in L	4.2	3.2	1.4	4.9	1.2	1.1
Extremum (−), %	7	5	4	4	3	4
Extremum (+), %	12	4	2	3	3	4

* See Table 1 footnote.

Table 3. Summary of the M_1, M_2, B_1, B_2 Parameters at $Ca > 1$

Speed, Ca	1.2	2.6	5.6	11.7	24	Overall Average (for all Ca)
Average Slopes (a)						
Upper, M_1	1.7	1.5	1.5	1.5	1.9	1.6
Lower, M_2	2.5	2.0	2.0	2.0	2.5	2.2
Upper Intercept, B_1						
At 30 depth (b)	17	14	9	8	12	—
At 15 depth	17	12	7	8	10	—
At 8 depth	6	7	7	5	5	—
At 4 depth	3	3(c)	5(c)	4	3	—
Lower Intercept, B_2						
At 30 depth (b)	6.4	6.8	5.8	5.6	5.8	6.1
At 15 depth	6.4	6.8	5.2	5.0	6.2	5.9
At 8 depth	3.8	3.9	4.0	3.7	3.9	3.9
At 4 depth	2.3	2.3(c)	2.6(c)	2.7	2.0	2.3

(a) Average of values at four depths. The individual slopes were not a function of depth, within the range and precision of this work.
(b) Depth in units of d/h_0, within a run-to-run variation of 30% in d/h_0.
(c) In these two runs, the entrainment checks had larger differences (> 10%) in Q, which indicates larger uncertainties in h_0 and in these parameters.

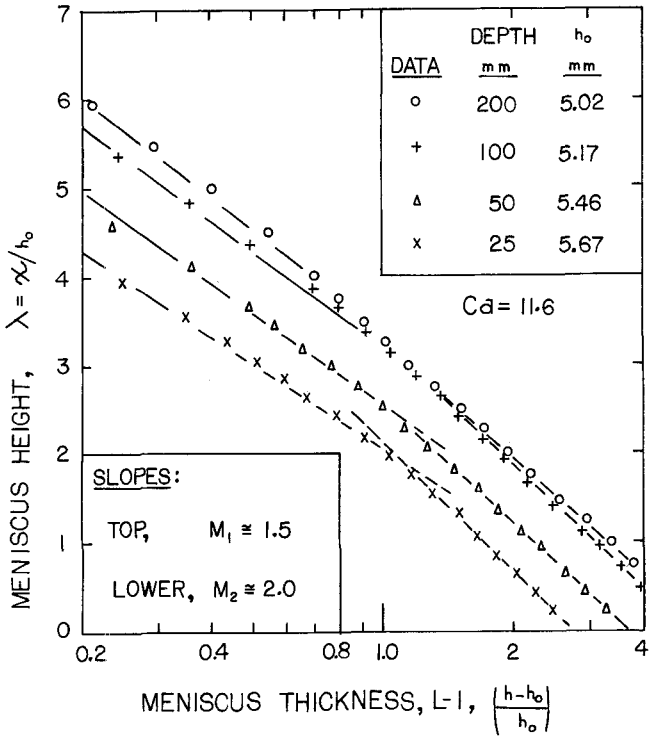

Fig. 3. Effect of bath depth on profiles at Ca near 12.

ters for shallow baths appear to be functions of both Ca and depth. For example, M_3 is not constant with depth at the same Ca (as is M_2), nor is B_3 constant with Ca at the same depth (as is B_2). Thus the Equation (4) approach is less suitable for comparing profiles than the two-equation approach used above.

However, the Equation (4) method does describe each of the 24 profiles precisely, is a complete, continuous profile, and has the proper limiting behaviors at both large and small λ. Therefore, it has an advantage for use as a boundary condition for flow fields.

DISCUSSION

Any plots of the L and λ parameters have the disadvantage that the static profile cannot be shown directly because of use of h_0 in both denominators. Static profiles can, however, be shown on plots of x versus ln $(h - h_0)$. Provision is made here to enable such a display, if desired; one should use the values of h_0 given in the tables.

To compare with Equation (4), a three-constant profile was sought. Study of the $L(\lambda)$ curvatures found in the region of L of 2 to 4 suggested another extension of Equation (1), which is

$$L = 1 + B_4 \exp(-\lambda/M_4)\,[1 + (\lambda/D)] \qquad (5)$$

Equation (5) was evaluated as follows. First the intercept B_4 was taken from data; thus it is nearly the same as B_2 given above. Next the term D was found to vary from about 10 to 30 but was taken as the constant value of 20 by smoothing for all 24 profiles. Third, the term M_4 was taken as a function of Ca only, by smoothing, and found to be 3.7, 2.9, 2.1, 2.1, 2.2, and 2.8 respectively at the increasing speeds shown in Table 1.

Comparison of maximum deviations of Equation (5) with Equation (4) indicates a similar precision. However, Equation (5) predicts a vanishing slope at large height, which is inconsistent with the top slopes for the upper region. Nevertheless, Equation (5) is a good approximation for the lower meniscus region and part of the upper meniscus and has the advantage of only three parameters at no loss in L precision.

SUMMARY

Precise values of twelve meniscus profiles and relevant conditions have been reported by use of analytical expressions which describe the data. (Tables 1 and 2 and Figures 1 and 2.) The influence of coating speed and bath depth on slopes and intercepts has been presented and discussed, based on 24 profiles. (Tables 2 and 3.) In addition, a complete profile of changing slope, tested with 24 profiles, has been found to describe L data within 10% in most cases. [Equation (4).] These expressions may be extendable to other geometries.

ACKNOWLEDGMENTS

This work was supported in part by the Eastman Kodak Co. The figures were drawn by Pradip Rao.

NOTATION

b = width of belt, mm
B = extrapolated intercept on λ $(L - 1)$ plot
B_1 = upper meniscus intercept, Equation (1)
B_2 = lower meniscus intercept, Equation (2)
B_3 = parameter, Equation (4)
B_4 = lower meniscus intercept, Equation (5)
Ca = capillary number, $Ca = U_w \mu/\sigma$
d = bath depth, mm
D = parameter, Equation (5)
h = meniscus thickness at any point, mm
h_0 = film thickness, constant thickness region, mm
L = meniscus thickness, dimensionless, h/h_0
M = slope on λ $(L - 1)$ plot
M_1 = upper meniscus slope, Equation (1)
M_2 = lower meniscus slope, Equation (2)
M_3 = parameter, Equation (4)
M_4 = parameter, Equation (5)
Q = flow rate of mass entrained, dimensionless, $(w/\rho b U_w)\ (\rho g/\mu U_w)^{0.5}$
Q_0 = flow rate calculated from h_0 data
Q_w = flow rate calculated from w data
t = temperature, °K
t_0 = reference temperature, 299.7°K.
T_0 = film thickness, dimensionless, $h_0\ (\rho g/\mu U_w)^{0.5}$
U_w = coating velocity of belt, mm/s
x = vertical coordinate, meniscus height above liquid level, mm
w = flow rate of mass entrained, g/s

Greek Letters

μ = liquid viscosity, N-s/m²
μ_0 = reference viscosity
ρ = liquid density, g/m³
λ = meniscus height, dimensionless, x/h_0
σ = surface tension of the liquid-air interface, N/m

LITERATURE CITED

Deryagin, D. V., and L. M. Levi, *Film Coating Theory*, Chapt. 2 and 4, Focal Press, New York (1964).

Lee, C. Y., and J. A. Tallmadge, "Meniscus Vortexing in Free Coating," *AIChE J.*, 18, 858 (1972a).

———., "Description of Meniscus Profiles in Free Coating," *ibid.*, 1077 (1972b).

Tallmadge, J. A., "Slope of the Upper Meniscus in Free Coating," *Chem. Eng. Sci.*, in press (1973).

Manuscript received August 21, 1972; revision received October 31, 1972; note accepted November 9, 1972.